

Fracture Detection in Pediatric Wrist Trauma X-ray Images Using YOLOv8 Algorithm

Rui-Yang Ju¹ and Weiming Cai^{2*}

¹Department of Electrical and Computer Engineering, Tamkang University, No.151, Yingzhuan Rd., Tamsui Dist., New Taipei City, 251301, Taiwan.

²Department of Hand and Foot Surgery, Jingjiang People's Hospital, No.28, Zhongzhou Rd., Jingjiang City, 214500, China.

*Corresponding author(s). E-mail(s): 1318746637@qq.com;
Contributing authors: jryjry1094791442@gmail.com;

Abstract

Hospital emergency departments frequently receive lots of bone fracture cases, with pediatric wrist trauma fracture accounting for the majority of them. Before pediatric surgeons perform surgery, they need to ask patients how the fracture occurred and analyze the fracture situation by interpreting X-ray images. The interpretation of X-ray images often requires a combination of techniques from radiologists and surgeons, which requires time-consuming specialized training. With the rise of deep learning in the field of computer vision, network models applying for fracture detection has become an important research topic. In this paper, YOLOv8 algorithm is used to train models on the GRAZPEDWRI-DX dataset, which includes X-ray images from 6,091 pediatric patients with wrist trauma. The experimental results show that YOLOv8 algorithm models have different advantages for different model sizes, with YOLOv8l model achieving the highest mean average precision (mAP 50) of 63.6%, and YOLOv8n model achieving the inference time of 67.4ms per X-ray image on one single CPU with low computing power. In this way, we create “Fracture Detection Using YOLOv8 App” to assist surgeons in interpreting X-ray images without the help of radiologists. Our implementation code is released at <https://github.com/RuiyangJu/Bone.Fracture.Detection.YOLOv8>.

Keywords: biomedical image processing, radiology, wrist trauma, X-ray, deep learning, fracture detection, YOLO

1 Introduction

In hospital emergency rooms, there are many patients who need to be examined by radiologists for fractures in various parts of the body, such as the wrist and arm. In general, bone fractures can be divided into open fractures (compound fractures), where the bone pierces the skin and becomes visible, and closed fractures (simple fractures), where the bone is broken but the skin remains intact. Before performing surgery, the surgeon needs to ask the patient how the fracture occurred and examine the patient for fracture. Fracture examinations are performed with three different devices, including X-ray, Magnetic Resonance Imaging (MRI), and Computed Tomography (CT) [1]. Considering the cost, X-ray is the most popular device among them.

Children are one of the major patient groups in bone fracture cases, with distal radius and distal ulna fractures accounting for the majority of wrist fractures in children and often occurring during adolescence [21][34]. X-ray images are usually analyzed by experienced radiologists in prestigious hospitals, while in some smaller hospitals, there are young and inexperienced surgeons who are unable to interpret the X-ray images correctly. The shortage of radiologists poses a threat to the possibility of immediate patient care [6][39]. Moreover, access to specialist reports is often more limited in some regions that are lagging behind in development [40]. According to the reports [31][10], the probability that x-ray images are misinterpreted to varying degrees is as high as 26%.

With the rapid development of deep learning, neural network models have been applied to the field of medical imaging [2][45][8][7]. As a popular research direction in the field of computer vision, object detection algorithms have been gradually used to detect bone fractures in recent years [12][22][27][3].

Object detection algorithms based on deep learning are mainly divided into one-stage algorithms and two-stage algorithms. Unlike the famous two-stage algorithm R-CNN [15] and its improved algorithms [14][38], one-stage algorithms usually generate the location and class probabilities of objects directly, which greatly improves the inference speed of the model. Among the one-stage algorithms, in addition to the classical model SSD [29], YOLO series algorithm models have better trade-offs in terms of inference speed and accuracy for real-time applications.

We train YOLOv8 [17] algorithm on the GRAZPEDWRI-DX dataset [32] for the fracture detection task and compare the performance of YOLOv8 algorithm models for different input image sizes and different model sizes.

The contributions of this paper are summarized as follows: (1) This work first applies YOLOv8 to the fracture detection task, and demonstrates that YOLOv8 algorithm possesses better generalization by evaluating the prediction results of the model for pediatric wrist trauma fractures. (2) We create an application for detecting pediatric wrist fractures, which aims to help pediatric surgeons to perform X-ray images interpretation without the assistance of radiologists, and to reduce the probability of X-ray images analysis errors.

2 Related Work

2.1 YOLO

YOLO series algorithms are designed to be applied in real-world scenarios, which constantly increase model inference speed while maintaining the accuracy of the model. YOLOv1 [35] set the input image size to $448 \times 448 \times 3$ and used GoogLeNet [44] to extract the feature maps, and then put the extracted feature maps on two fully connected layers to obtain the final output. YOLOv1 used direct regression, which greatly reduced the computation of the model and improved the model inference speed. YOLOv2 [36] used DarkNet-19 as the backbone network and added a passthrough layer to combine high and low level semantic information, which improved the ability of the model to detect small objects. YOLOv3 [37] proposed a modified backbone network DarkNet-53 and added the concept of Feature Pyramid Networks (FPN) [25] to detect objects using multi-scale feature maps. YOLOv4 [4] combined Cross Stage Partial (CSP) [47] and DarkNet-53 to propose CSPDarkNet-53, which enabled the model to obtain richer gradient fusion information. In addition, YOLOv4 used Spatial Pyramid Pooling (SSP) [20] to expand the receptive field and added Path Aggregation Network (PAN) [28] to the Neck of the model, which reduced the computation of the model. YOLOv5 [16] used Spatial Pyramid Pooling - Fast (SPPF) [20] to replace the SPP architecture and added the Focus module to improve the model performance. YOLOv6 [24] used EfficientRep [49] as the backbone network and designed Rep-PAN based on PAN [28] and Rep [9], which was added to the Neck of the model. Wang *et al.* [24] received inspiration from YOLOX [13] to use decoupling operations for the Head in YOLOv6 algorithm architecture. YOLOv7 [46] proposed planned re-parameterized convolution module and the concept of model scaling and expansion to enable the model to use the parameters more efficiently.

2.2 Fracture Detection

In recent years, researchers have applied neural networks to clinical bone image data for fracture detection tasks. Guan *et al.* [18] obtained average precision of 82.1% on 3,842 thigh fracture X-ray images using the Dilated Convolutional Feature Pyramid Network (DCFPN). Guan *et al.* [19] used R-CNN [15] for fracture detection on Musculoskeletal-Radiograph dataset (MURA) and obtained the average precision of 62.04%. Wang *et al.* [48] used ParalleNet with TripleNet as the backbone network for fracture detection on 3,842 thigh fracture X-ray images. Ma and Luo [30] took 1,052 bone images as the dataset, used Faster R-CNN [38] for fracture detection in a part, and used CrackNet model for fracture classification on the whole dataset. Wu *et al.* [50] used ResNeXt101 and FPN [25] on the Feature Ambiguity Mitigate Operator dataset (FAMO) for fracture detection. Qi *et al.* [33] used Fast R-CNN [14] with ResNet50 as the backbone network to detect nine different types of fractures on 2,333 fracture X-ray images. Sha *et al.* [43][42] used YOLOv2 [36] and Faster R-CNN [38]

models for fracture detection on 5,134 CT images of spine fractures, respectively. Xue *et al.* [51] used Faster R-CNN [38] model for fracture detection on 3,067 hand fracture X-ray images and obtained the average precision of 70.0%. Most of the work used R-CNN series models for fracture detection, and there are no researches using YOLOv8 model for fracture detection.

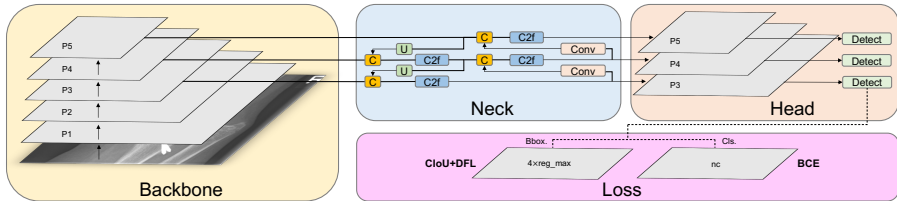


Fig. 1 The overall network model architecture of YOLOv8 algorithm.

3 Proposed Method

YOLOv8 algorithm architecture consists of Backbone, Neck, Head, and Loss, as shown in Fig. 1. In the following subsections, we introduce the design concepts of each part of the architecture in detail.

3.1 Backbone

The Backbone part of YOLOv8 uses the concept of Cross Stage Partial (CSP) [47] to split the feature map into two parts, where Part 1 uses convolution operations, and Part 2 is concatenated with the output of the convolution operations of the previous part. CSP architecture improves the learning ability of the Convolutional Neural Network (CNN) and reduces the computational effort of the network model. Unlike C3 module used in YOLOv5 [16], YOLOv8 uses C2f module instead. C3 module consists of 3 ConvModule and n BottleNeck, while C2f module consists of 2 ConvModule and n BottleNeck connected through Split and Concat. As shown in Fig. 2, ConvModule consists of *Conv-BN-SiLU*. C2f module is proposed by combining C3 module and the concept of ELAN in YOLOv7 [46], which enables YOLOv8 to obtain richer gradient flow information while ensuring the lightweight of the algorithm model.

In addition, to further reduce the computational effort of the model, YOLOv8 algorithm reduces the number of blocks in each stage from 3,6,9,3 used in YOLOv5 to 3,6,6,3. And in Stage 4, YOLOv8 follows the SPPF module used in YOLOv5. As shown in Fig. 2, SPPF is improved from SPP [20] to enhance the inference speed of the model.

3.2 Neck

In general, when network is deeper, more feature information is obtained and the prediction result of the object is better. However, deeper networks lead to

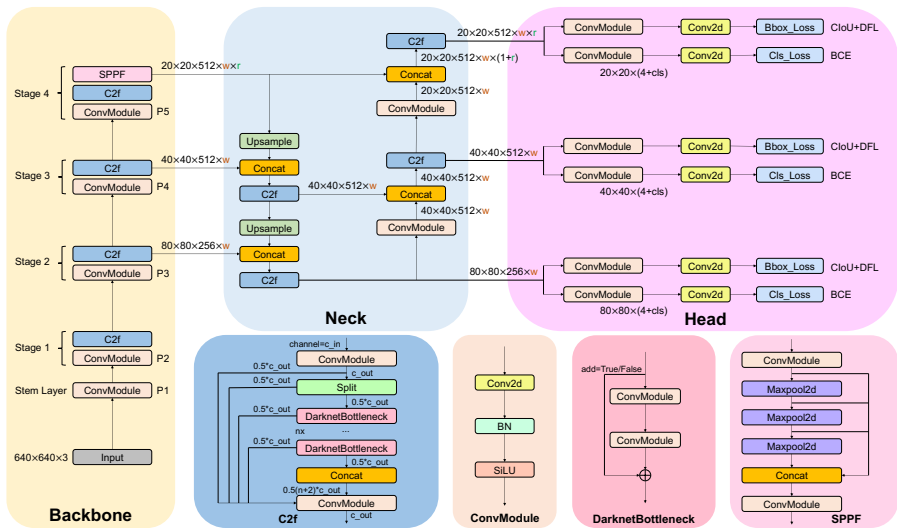


Fig. 2 Detailed illustration of each module in YOLOv8 algorithm architecture.

reduction of the object location information. For small objects, too many convolution operations result in information loss, so multi-scale fusion of features using FPN [25] and PAN [28] architectures is necessary. As shown in Fig. 2, the Neck part of the architecture uses multi-scale feature fusion of images, the upper features obtain more information because of more network layers, while the lower features lose less location information because of fewer convolution layers.

YOLOv5 [16] uses FPN structure to make the bottom feature map contain more feature information by up-sampling from top to bottom, and PAN structure to make the top feature contain more position information by down-sampling from bottom to top. These two feature outputs finally merge to ensure accurate prediction for images of different sizes. YOLOv8 follows FPN and PAN structures and removes the convolution operations in the up-sampling stage.

3.3 Head

Different from YOLOv5 [16] using the coupled head, YOLOv8 uses the decoupled head instead, separating the classification and detection head. As shown in Fig. 2, YOLOv8 removes the objectness branch and keeps only the classification and regression branches. Anchor-Base first presets a large number of anchors in the image, calculates the four offsets of the regression object with respect to the anchors, and finally corrects the exact object position using the corresponding anchors and offsets. YOLOv8 replaces Anchor-Base with Anchor-Free, which locates the object by its center, and then predicts the distance from the center to the bounding box.

3.4 Loss

For positive and negative sample assignment, YOLOv8 algorithm uses the Task Aligned Assigner of TOOD [11] to select positive samples based on the weighted scores of classification and regression, as shown in the following equation:

$$t = s^\alpha \times u^\beta, \quad (1)$$

where s is the predicted score corresponding to the labeled class, and u is the IoU of the prediction and the ground truth bounding box. YOLOv8 algorithm has classification and regression branches, where classification branch uses BCE Loss, and the equation is shown below:

$$Loss_n = -w [y_n \cdot \log x_n + (1 - y_n) \cdot \log (1 - x_n)], \quad (2)$$

where w is the weight, y_n is the labeled value, and x_n is the predicted value of the algorithm model. And the regression branch uses Distribute Focal Loss (DFL) and CIoU Loss. The purpose of DFL is to focus on expanding the probability of the value around the object y , and its equation is shown as follows:

$$DFL(\mathcal{S}_n, \mathcal{S}_{n+1}) = -((y_{n+1} - y) \log(\mathcal{S}_n) + (y - y_n) \log(\mathcal{S}_{n+1})), \quad (3)$$

$$\mathcal{S}_n = \frac{y_{n+1} - y}{y_{n+1} - y_n}, \mathcal{S}_{n+1} = \frac{y - y_n}{y_{n+1} - y_n}. \quad (4)$$

CIoU Loss adds an influence factor to DIoU Loss [52] by considering the aspect ratio of the prediction and the ground truth bounding box, which is shown below:

$$CIoU_{Loss} = 1 - CIoU = 1 - \left(IoU - \frac{Distance_2^2}{Distance_C^2} - \frac{\nu^2}{(1 - IoU) + \nu} \right), \quad (5)$$

where ν is the parameter to measure the consistency of aspect ratio, we define as follows:

$$\nu = \frac{4}{\pi^2} \left(\arctan \frac{w^{gt}}{h^{gt}} - \arctan \frac{w^p}{h^p} \right)^2. \quad (6)$$

4 Experiments

4.1 Dataset

GRAZPEDWRI-DX [32] is a public dataset provided by the Medical University of Graz, which contains 20,327 pediatric wrist trauma X-ray images involving 6,091 patients. These images have been collected by several pediatric radiologists at the Department for Pediatric Surgery of the University Hospital Graz between 2008 and 2018, and are annotated in 9 different classes by placing bounding boxes, as shown in Table 1.

Table 1 The classes of GRAZPEDWRI-DX dataset

| The classes of GRAZPEDWRI-DX dataset | | |
|--------------------------------------|-----------------------|---------------------------------|
| boneanomaly (276 boxes) | metal (818 boxes) | softtissue (464 boxes) |
| pronatorsign (567 boxes) | text (23722 boxes) | bonelesion (45 boxes) |
| fracture (18090 boxes) | foreignbody (8 boxes) | periostealreaction (3453 boxes) |

We randomly divide the GRAZPEDWRI-DX dataset into training set, validation set and test set, and the number of images in these three sets are about 70%, 20% and 10% of the original dataset, respectively. For the experiments in Section 4.4, our training set contains 14,204 images (69.88%), the validation set contains 4,094 images (20.14%), and the test set contains 2,029 images (9.98%). Readers can find the code for splitting the dataset in our GitHub link, but note that each split is random and not reproducible.

4.2 Evaluation Metric

4.2.1 Intersection over Union (IoU)

Intersection over Union (IoU) is a classical metric for evaluating the performance of the algorithm in object detection tasks. IoU is the ratio of the overlap and union of the generated candidate and the ground truth bounding box, representing the intersection of these two bounding boxes. And the equation is as follows:

$$IoU = \frac{area(C) \cap area(G)}{area(C) \cup area(G)}, \quad (7)$$

where C represents the candidate bounding box and G represents the ground truth bounding box in which the object is located. The algorithm performance gets better as the IoU metric value increases, with higher IoU values representing less difference between the candidate and the ground truth bounding box.

4.2.2 Precision-Recall Curve

Precision-Recall Curve (P-R Curve) [5] is a curve with Recall as the x-axis and Precision as the y-axis. Each point represents a different threshold value, and all points are connected as a curve. The Recall (R) and Precision (P) are calculated according to the following equations:

$$Precision = \frac{T_P}{T_P + F_P}, Recall = \frac{T_P}{T_P + F_N}, \quad (8)$$

where True Positive (T_P) means the prediction result is positive class and is judged to be true; False Positive (F_P) means the prediction result is positive class but is judged to be false; False Negative (F_N) means the prediction result is negative class but is judged to be false.

4.2.3 F1-score

F-score is a common metric for evaluating the accuracy of the algorithm, which reflects the performance of the algorithm in a balanced way by considering both Precision and Recall. The equation of F-score is shown below:

$$F - score = \frac{(1 + \beta^2) precision \times recall}{\beta^2 precision + recall} \quad (9)$$

In general, the weights of Precision and Recall in F1-score are the same when $\beta=1$, representing the harmonic mean of Precision and Recall, the equation of which is shown below:

$$F_1 = \frac{2PR}{P + R} = \frac{2T_P}{2T_P + F_P + F_N} \quad (10)$$

4.2.4 Mean Average Precision (mAP)

Mean Average Precision (mAP) is one of the most popular evaluation metrics used in object detection tasks to measure the performance of the algorithm in all classes. In Section 4.4 of this paper, we use mAP 50 and mAP 50-95 to evaluate the performance of different algorithms. mAP 50 represents the average precision for all classes at IoU of 0.5, while mAP 50-95 represents the average precision for all classes from IoU of 0.5 to IoU of 0.95, with step size of 0.05.

4.3 Experiment Setup

In the process of training all models, we use YOLOv8 models trained on COCO val2017 dataset [26] as pre-trained models. According to the experimental data provided by Ultralytics [16][17], the number of epochs used for YOLOv5 training was 300, while YOLOv8 increased the number of epochs to 500. Since we use pre-trained models, we initially set the total number of epochs to 200 and set the patience to 50, which means that if no observable improvement after waiting for 50 epochs, the training will stop early. When training YOLOv8m, we find that the model training stop early at epoch 112 and the best performance is at epoch 62. To save computing resources, we change the number of epochs for all model training to 100.

For the hyperparameters of the model training, according to the suggestion of Glenn [17], the Adam [23] optimizer is more suitable for training small custom dataset, while the SGD [41] optimizer always performs better on large datasets. We use Adam and SGD optimizers to train YOLOv8 models separately, and compare the effects of the two optimizers for model training, and the comparison results are shown in Table 2.

For the experiments in Section 4.4, we choose Adam [23] as the optimizer, and the weight decay of the optimizer is set to 5×10^{-4} , while the initial learning rate is set to 1×10^{-3} . In addition, we set the input image size to 640 and 1024, train different models on GeForce RTX 3080Ti 12GB and GeForce RTX 3090

Table 2 Comparison of model performance of YOLOv8s and YOLOv8m trained on the GRAZPEDWRI-DX dataset using SGD and Adam optimizers.

| Model | size (pixels) | Optimizer ¹ | Best Eepoch | mAP ^{val} 50 | mAP ^{val} 50-95 | Speed GPU 3080Ti (ms) |
|---------|------------------|------------------------|-------------|--------------------------|-----------------------------|-----------------------------|
| YOLOv8s | 640 | SGD | 56 | 0.631 | 0.399 | 4.4 |
| YOLOv8s | 640 | Adam | 57 | 0.604 | 0.383 | 4.3 |
| YOLOv8s | 1024 | SGD | 36 | 0.623 | 0.395 | 5.4 |
| YOLOv8s | 1024 | Adam | 47 | 0.622 | 0.399 | 4.9 |
| YOLOv8m | 640 | SGD | 52 | 0.611 | 0.396 | 4.9 |
| YOLOv8m | 640 | Adam | 62 | 0.631 | 0.403 | 5.5 |
| YOLOv8m | 1024 | SGD | 35 | 0.614 | 0.402 | 9.9 |
| YOLOv8m | 1024 | Adam | 70 | 0.614 | 0.399 | 10.0 |

¹ For training with the SGD optimizer, the initial learning rate is 1×10^{-2} . For training with the Adam optimizer, the initial learning rate is 1×10^{-3} .

24GB, respectively, and both batch size are set to 16. We train the models on Python 3.8 and PyTorch 1.8.2, and recommend that readers use Python 3.7 or higher and PyTorch 1.7 or higher for training. It is worth noting that due to GPU memory limitations, when training YOLOv8l model, GeForce RTX 3090 24GB used 4 worker threads to load data, and GeForce RTX 3080Ti 12GB used 3 worker threads to load data. Therefore, using GPUs with larger memory and more computing power can effectively increase the speed of model training.

4.4 Experimental Results

To evaluate the feasibility of YOLOv8 models for fracture detection in a real-world hospital diagnostic scenario, this section focuses on comparing the mean average precision (mAP 50) and inference time of different models.

To overcome the effect of the choice of optimizer on model performance during training, we compare models trained using the SGD [41] optimizer recommended by Glenn [17] and another popular optimizer Adam [23]. As shown in Table 2, training the model using the SGD optimizer requires less number of weight updates. For YOLOv8m model with the input image size of 1024, the model trained with the SGD optimizer achieves the best model performance at the 35th epoch, while for the model trained with the Adam optimizer, the best model performance is at the 75th epoch. When the input image size is 640, the mAP 50 for the YOLOv8s model trained with the SGD optimizer is better at 0.631. The difference in inference time for the models trained with different optimizers is less, with a maximum difference of 0.6ms.

In the fracture detection task, to evaluate the effect of different input image sizes on model performance, we obtain Precision-Recall Curve (P-R Curve) and F1-Confidence Curve for YOLOv8l with input image size of 640 and 1024. As shown in Fig. 3, in P-R Curve, the curve of the overall class of the model with input image size of 1024 contains a larger area and its F1 value is larger, which demonstrates that the increase in input image size has a positive effect on the model performance.

Table 3 Comparison of model performance of different sizes of YOLOv8.

| Model | size (pixels) | mAP ^{val} | | Speed | | params (M) | FLOPs (B) |
|---------|------------------|--------------------|-------|-------------------------------|---------------------------------|---------------|--------------|
| | | 50 | 50-95 | CPU ONNX ¹ (ms) | GPU 3080Ti ² (ms) | | |
| YOLOv8n | 640 | 0.601 | 0.374 | 67.4 | 2.9 | 3.0 | 8.1 |
| YOLOv8s | 640 | 0.604 | 0.383 | 191.5 | 4.3 | 11.1 | 28.5 |
| YOLOv8m | 640 | 0.631 | 0.403 | 536.4 | 5.5 | 25.8 | 78.7 |
| YOLOv8l | 640 | 0.620 | 0.403 | 1006.3 | 7.4 | 43.6 | 164.9 |
| YOLOv8n | 1024 | 0.605 | 0.387 | 212.1 | 3.3 | 3.0 | 8.1 |
| YOLOv8s | 1024 | 0.622 | 0.399 | 519.5 | 4.9 | 11.1 | 28.5 |
| YOLOv8m | 1024 | 0.614 | 0.399 | 1521.5 | 10.0 | 25.8 | 78.7 |
| YOLOv8l | 1024 | 0.636 | 0.404 | 2671.1 | 15.1 | 43.6 | 164.9 |

¹ Speed CPU ONNX is the total time of validation per image on the CPU Intel Core i5, including preprocessing time, inference time and post processing time.

² Speed GPU 3080Ti is the total time of validation per image on the GPU NVIDIA GeForce RTX 3080Ti, including preprocessing time, inference time and post processing time.

Table 4 Detailed data for each class evaluated on YOLOv8l model with the input image size of 1024.

| Class | size (pixels) | Images | Instances | Precision | Recall | mAP ^{val} | |
|--------------------|------------------|--------|-----------|-----------|--------|--------------------|-------|
| | | | | | | 50 | 50-95 |
| overall | 1024 | 4094 | 9613 | 0.600 | 0.679 | 0.636 | 0.404 |
| boneanomaly | 1024 | 4094 | 53 | 0.284 | 0.150 | 0.084 | 0.03 |
| bonelesion | 1024 | 4094 | 8 | 0.488 | 0.597 | 0.531 | 0.291 |
| fracture | 1024 | 4094 | 3740 | 0.864 | 0.918 | 0.945 | 0.567 |
| metal | 1024 | 4094 | 168 | 0.771 | 0.899 | 0.901 | 0.710 |
| periostealreaction | 1024 | 4094 | 697 | 0.596 | 0.732 | 0.722 | 0.376 |
| pronatorsign | 1024 | 4094 | 104 | 0.472 | 0.846 | 0.663 | 0.368 |
| softtissue | 1024 | 4094 | 89 | 0.370 | 0.303 | 0.256 | 0.132 |
| text | 1024 | 4094 | 4754 | 0.955 | 0.984 | 0.990 | 0.753 |

In this paper, YOLOv8 model is used for the fracture detection application. In the application deployed on the personal computer, we use YOLOv8l algorithm model for fracture detection, the X-ray images manually labeled by the radiologist and the output images predicted using the network model are shown in Fig. 4. As shown in Table 3, the larger size of YOLOv8 model has the higher mAP 50 of 0.636. However, the increase in model size results in longer inference time, especially on low computational power CPU. Therefore, smaller models should be chosen for deployment on mobile phones, such as YOLOv8n with the inference time of 67.4ms. For applications on computers with strong computational power, we recommend using larger models to obtain more accurate predictions.

In order to prepare for the future improvement of the model performance, we calculate the experimental data for each class respectively, as shown in Table 4. Among all classes, YOLOv8 model has better accuracy in detecting fracture, metal and text, with mAP 50 of each above 0.9. On the opposite, the detection ability of boneanomaly and softtissue is poor, with mAP 50 of 0.084 and 0.256, respectively. Therefore, in future works, more information about boneanomaly and softtissue should be given to the model to learn.

4.5 Application

After completing the model training, we export YOLOv8l model with 640 input image size to ONNX format and use PySide6 to create the Graphical User Interface (GUI) application. PySide (Qt for Python) is a Python library for creating GUI applications using the Qt toolkit. PySide6 is the Qt6-based version of Python GUI library PySide from the Qt Company. As shown in Fig. 5, we create a GUI application named “Fracture Detection Using YOLOv8 App”, and the icons in the application refer to the icons in Flaticon. Users can open images, make predictions, and save predictions in our application, which is designed to assist surgeons in observing bone fractures of pediatric wrists.

5 Conclusion

In this paper, we propose an application named “Fracture Detection Using YOLOv8 App” to detect fractures in pediatric wrist trauma X-ray images by using neural network models. As the latest algorithm in YOLO series, there are relatively few researches using YOLOv8 algorithm models for detection tasks, and this paper demonstrates YOLOv8 algorithm has better generalization. For the dataset, we randomly divide 20,327 pediatric wrist trauma X-ray images from 6,091 patients into training set, test set, and validation set. We hope that the newly proposed application will help pediatric surgeons interpret the X-ray images, reduce the probability of error and provide more correct information for fracture surgery.

6 Declarations

6.1 Funding

The authors did not receive support from any organization for the submitted work.

6.2 Competing interests

The authors have no financial or proprietary interests in any material discussed in this article.

6.3 Ethics approval

We declare that all pediatric wrist trauma fracture X-ray images used in this research were from GRAZPEDWRI-DX, which is a public dataset.

References

- [1] Fractures, health, hopkins medicine. <https://www.hopkinsmedicine.org/health/conditions-and-diseases/fractures> (2021)

- [2] Adams, S.J., Henderson, R.D., Yi, X., Babyn, P.: Artificial intelligence solutions for analysis of x-ray images. *Canadian Association of Radiologists Journal* **72**(1), 60–72 (2021)
- [3] Blüthgen, C., Becker, A.S., de Martini, I.V., Meier, A., Martini, K., Frauenfelder, T.: Detection and localization of distal radius fractures: Deep learning system versus radiologists. *European journal of radiology* **126**, 108,925 (2020)
- [4] Bochkovskiy, A., Wang, C.Y., Liao, H.Y.M.: Yolov4: Optimal speed and accuracy of object detection. arXiv preprint arXiv:2004.10934 (2020)
- [5] Boyd, K., Eng, K.H., Page, C.D.: Area under the precision-recall curve: point estimates and confidence intervals. In: *Machine Learning and Knowledge Discovery in Databases: European Conference, ECML PKDD 2013, Prague, Czech Republic, September 23-27, 2013, Proceedings, Part III* 13, pp. 451–466. Springer (2013)
- [6] Burki, T.K.: Shortfall of consultant clinical radiologists in the uk. *The Lancet Oncology* **19**(10), e518 (2018)
- [7] Choi, J.W., Cho, Y.J., Lee, S., Lee, J., Lee, S., Choi, Y.H., Cheon, J.E., Ha, J.Y.: Using a dual-input convolutional neural network for automated detection of pediatric supracondylar fracture on conventional radiography. *Investigative radiology* **55**(2), 101–110 (2020)
- [8] Chung, S.W., Han, S.S., Lee, J.W., Oh, K.S., Kim, N.R., Yoon, J.P., Kim, J.Y., Moon, S.H., Kwon, J., Lee, H.J., et al.: Automated detection and classification of the proximal humerus fracture by using deep learning algorithm. *Acta orthopaedica* **89**(4), 468–473 (2018)
- [9] Ding, X., Zhang, X., Ma, N., Han, J., Ding, G., Sun, J.: Repvgg: Making vgg-style convnets great again. In: *Proceedings of the IEEE/CVF conference on computer vision and pattern recognition*, pp. 13,733–13,742 (2021)
- [10] Erhan, E., Kara, P., Oyar, O., Unluer, E.: Overlooked extremity fractures in the emergency department. *Ulus Travma Acil Cerrahi Derg* **19**(1), 25–8 (2013)
- [11] Feng, C., Zhong, Y., Gao, Y., Scott, M.R., Huang, W.: Toood: Task-aligned one-stage object detection. In: *2021 IEEE/CVF International Conference on Computer Vision (ICCV)*, pp. 3490–3499. IEEE Computer Society (2021)
- [12] Gan, K., Xu, D., Lin, Y., Shen, Y., Zhang, T., Hu, K., Zhou, K., Bi, M., Pan, L., Wu, W., et al.: Artificial intelligence detection of distal radius

- fractures: a comparison between the convolutional neural network and professional assessments. *Acta orthopaedica* **90**(4), 394–400 (2019)
- [13] Ge, Z., Liu, S., Wang, F., Li, Z., Sun, J.: Yolox: Exceeding yolo series in 2021. arXiv preprint arXiv:2107.08430 (2021)
- [14] Girshick, R.: Fast r-cnn. In: Proceedings of the IEEE international conference on computer vision, pp. 1440–1448 (2015)
- [15] Girshick, R., Donahue, J., Darrell, T., Malik, J.: Rich feature hierarchies for accurate object detection and semantic segmentation. In: Proceedings of the IEEE conference on computer vision and pattern recognition, pp. 580–587 (2014)
- [16] Glenn, J.: Ultralytics yolov5. <https://github.com/ultralytics/yolov5> (2022)
- [17] Glenn, J.: Ultralytics yolov8. <https://github.com/ultralytics/ultralytics> (2023)
- [18] Guan, B., Yao, J., Zhang, G., Wang, X.: Thigh fracture detection using deep learning method based on new dilated convolutional feature pyramid network. *Pattern Recognition Letters* **125**, 521–526 (2019)
- [19] Guan, B., Zhang, G., Yao, J., Wang, X., Wang, M.: Arm fracture detection in x-rays based on improved deep convolutional neural network. *Computers & Electrical Engineering* **81**, 106,530 (2020)
- [20] He, K., Zhang, X., Ren, S., Sun, J.: Spatial pyramid pooling in deep convolutional networks for visual recognition. *IEEE transactions on pattern analysis and machine intelligence* **37**(9), 1904–1916 (2015)
- [21] Hedström, E.M., Svensson, O., Bergström, U., Michno, P.: Epidemiology of fractures in children and adolescents: Increased incidence over the past decade: a population-based study from northern sweden. *Acta orthopaedica* **81**(1), 148–153 (2010)
- [22] Kim, D., MacKinnon, T.: Artificial intelligence in fracture detection: transfer learning from deep convolutional neural networks. *Clinical radiology* **73**(5), 439–445 (2018)
- [23] Kingma, D.P., Ba, J.: Adam: A method for stochastic optimization. arXiv preprint arXiv:1412.6980 (2014)
- [24] Li, C., Li, L., Jiang, H., Weng, K., Geng, Y., Li, L., Ke, Z., Li, Q., Cheng, M., Nie, W., et al.: Yolov6: A single-stage object detection framework for industrial applications. arXiv preprint arXiv:2209.02976 (2022)

- [25] Lin, T.Y., Dollár, P., Girshick, R., He, K., Hariharan, B., Belongie, S.: Feature pyramid networks for object detection. In: Proceedings of the IEEE conference on computer vision and pattern recognition, pp. 2117–2125 (2017)
- [26] Lin, T.Y., Maire, M., Belongie, S., Hays, J., Perona, P., Ramanan, D., Dollár, P., Zitnick, C.L.: Microsoft coco: Common objects in context. In: Computer Vision–ECCV 2014: 13th European Conference, Zurich, Switzerland, September 6–12, 2014, Proceedings, Part V 13, pp. 740–755. Springer (2014)
- [27] Lindsey, R., Daluiski, A., Chopra, S., Lachapelle, A., Mozer, M., Sicular, S., Hanel, D., Gardner, M., Gupta, A., Hotchkiss, R., et al.: Deep neural network improves fracture detection by clinicians. Proceedings of the National Academy of Sciences **115**(45), 11,591–11,596 (2018)
- [28] Liu, S., Qi, L., Qin, H., Shi, J., Jia, J.: Path aggregation network for instance segmentation. In: Proceedings of the IEEE conference on computer vision and pattern recognition, pp. 8759–8768 (2018)
- [29] Liu, W., Anguelov, D., Erhan, D., Szegedy, C., Reed, S., Fu, C.Y., Berg, A.C.: Ssd: Single shot multibox detector. In: Computer Vision–ECCV 2016: 14th European Conference, Amsterdam, The Netherlands, October 11–14, 2016, Proceedings, Part I 14, pp. 21–37. Springer (2016)
- [30] Ma, Y., Luo, Y.: Bone fracture detection through the two-stage system of crack-sensitive convolutional neural network. Informatics in Medicine Unlocked **22**, 100,452 (2021)
- [31] Mounts, J., Clingenpeel, J., McGuire, E., Byers, E., Kireeva, Y.: Most frequently missed fractures in the emergency department. Clinical pediatrics **50**(3), 183–186 (2011)
- [32] Nagy, E., Janisch, M., Hrzić, F., Sorantin, E., Tschauner, S.: A pediatric wrist trauma x-ray dataset (grazpedwri-dx) for machine learning. Scientific Data **9**(1), 222 (2022)
- [33] Qi, Y., Zhao, J., Shi, Y., Zuo, G., Zhang, H., Long, Y., Wang, F., Wang, W.: Ground truth annotated femoral x-ray image dataset and object detection based method for fracture types classification. IEEE Access **8**, 189,436–189,444 (2020)
- [34] Randsborg, P.H., Gulbrandsen, P., Benth, J.Š., Sivertsen, E.A., Hammer, O.L., Fuglesang, H.F., Årøen, A.: Fractures in children: epidemiology and activity-specific fracture rates. JBJS **95**(7), e42 (2013)

- [35] Redmon, J., Divvala, S., Girshick, R., Farhadi, A.: You only look once: Unified, real-time object detection. In: Proceedings of the IEEE conference on computer vision and pattern recognition, pp. 779–788 (2016)
- [36] Redmon, J., Farhadi, A.: Yolo9000: better, faster, stronger. In: Proceedings of the IEEE conference on computer vision and pattern recognition, pp. 7263–7271 (2017)
- [37] Redmon, J., Farhadi, A.: Yolov3: An incremental improvement. arXiv preprint arXiv:1804.02767 (2018)
- [38] Ren, S., He, K., Girshick, R., Sun, J.: Faster r-cnn: Towards real-time object detection with region proposal networks. *Advances in neural information processing systems* **28** (2015)
- [39] Rimmer, A.: Radiologist shortage leaves patient care at risk, warns royal college. *BMJ: British Medical Journal (Online)* **359** (2017)
- [40] Rosman, D., Nshizirungu, J., Rudakemwa, E., Moshi, C., de Dieu Tuyisenge, J., Uwimana, E., Kalisa, L.: Imaging in the land of 1000 hills: Rwanda radiology country report. *Journal of Global Radiology* **1**(1) (2015)
- [41] Ruder, S.: An overview of gradient descent optimization algorithms. arXiv preprint arXiv:1609.04747 (2016)
- [42] Sha, G., Wu, J., Yu, B.: Detection of spinal fracture lesions based on improved faster-rcnn. In: 2020 IEEE International Conference on Artificial Intelligence and Information Systems (ICAIS), pp. 29–32. IEEE (2020)
- [43] Sha, G., Wu, J., Yu, B.: Detection of spinal fracture lesions based on improved yolov2. In: 2020 IEEE International Conference on Artificial Intelligence and Computer Applications (ICAICA), pp. 235–238. IEEE (2020)
- [44] Szegedy, C., Liu, W., Jia, Y., Sermanet, P., Reed, S., Anguelov, D., Erhan, D., Vanhoucke, V., Rabinovich, A.: Going deeper with convolutions. In: Proceedings of the IEEE conference on computer vision and pattern recognition, pp. 1–9 (2015)
- [45] Tanzi, L., Vezzetti, E., Moreno, R., Aprato, A., Audisio, A., Massè, A.: Hierarchical fracture classification of proximal femur x-ray images using a multistage deep learning approach. *European journal of radiology* **133**, 109,373 (2020)

- [46] Wang, C.Y., Bochkovskiy, A., Liao, H.Y.M.: Yolov7: Trainable bag-of-freebies sets new state-of-the-art for real-time object detectors. arXiv preprint arXiv:2207.02696 (2022)
- [47] Wang, C.Y., Liao, H.Y.M., Wu, Y.H., Chen, P.Y., Hsieh, J.W., Yeh, I.H.: Cspnet: A new backbone that can enhance learning capability of cnn. In: Proceedings of the IEEE/CVF conference on computer vision and pattern recognition workshops, pp. 390–391 (2020)
- [48] Wang, M., Yao, J., Zhang, G., Guan, B., Wang, X., Zhang, Y.: Parallelnet: Multiple backbone network for detection tasks on thigh bone fracture. *Multimedia Systems* pp. 1–10 (2021)
- [49] Weng, K., Chu, X., Xu, X., Huang, J., Wei, X.: Efficientrep: An efficient repvgg-style convnets with hardware-aware neural network design. arXiv preprint arXiv:2302.00386 (2023)
- [50] Wu, H.Z., Yan, L.F., Liu, X.Q., Yu, Y.Z., Geng, Z.J., Wu, W.J., Han, C.Q., Guo, Y.Q., Gao, B.L.: The feature ambiguity mitigate operator model helps improve bone fracture detection on x-ray radiograph. *Scientific Reports* **11**(1), 1–10 (2021)
- [51] Xue, L., Yan, W., Luo, P., Zhang, X., Chaikovska, T., Liu, K., Gao, W., Yang, K.: Detection and localization of hand fractures based on ga_faster r-cnn. *Alexandria Engineering Journal* **60**(5), 4555–4562 (2021)
- [52] Zheng, Z., Wang, P., Liu, W., Li, J., Ye, R., Ren, D.: Distance-iou loss: Faster and better learning for bounding box regression. In: Proceedings of the AAAI conference on artificial intelligence, vol. 34, pp. 12,993–13,000 (2020)

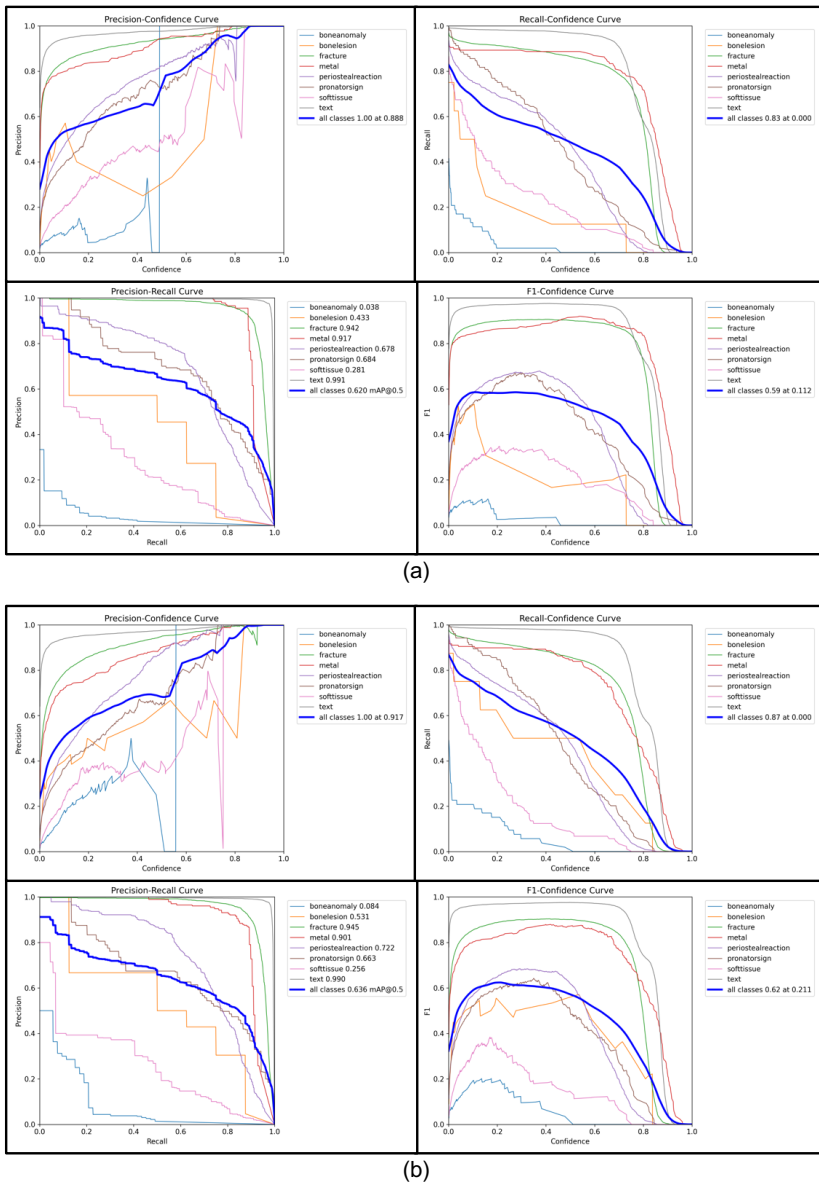


Fig. 3 Model training details of YOLOv8l on the GRAZPEDWRI-DX dataset. (a) the input image size of YOLOv8l is 640, (b) the input image size of YOLOv8l is 1024.

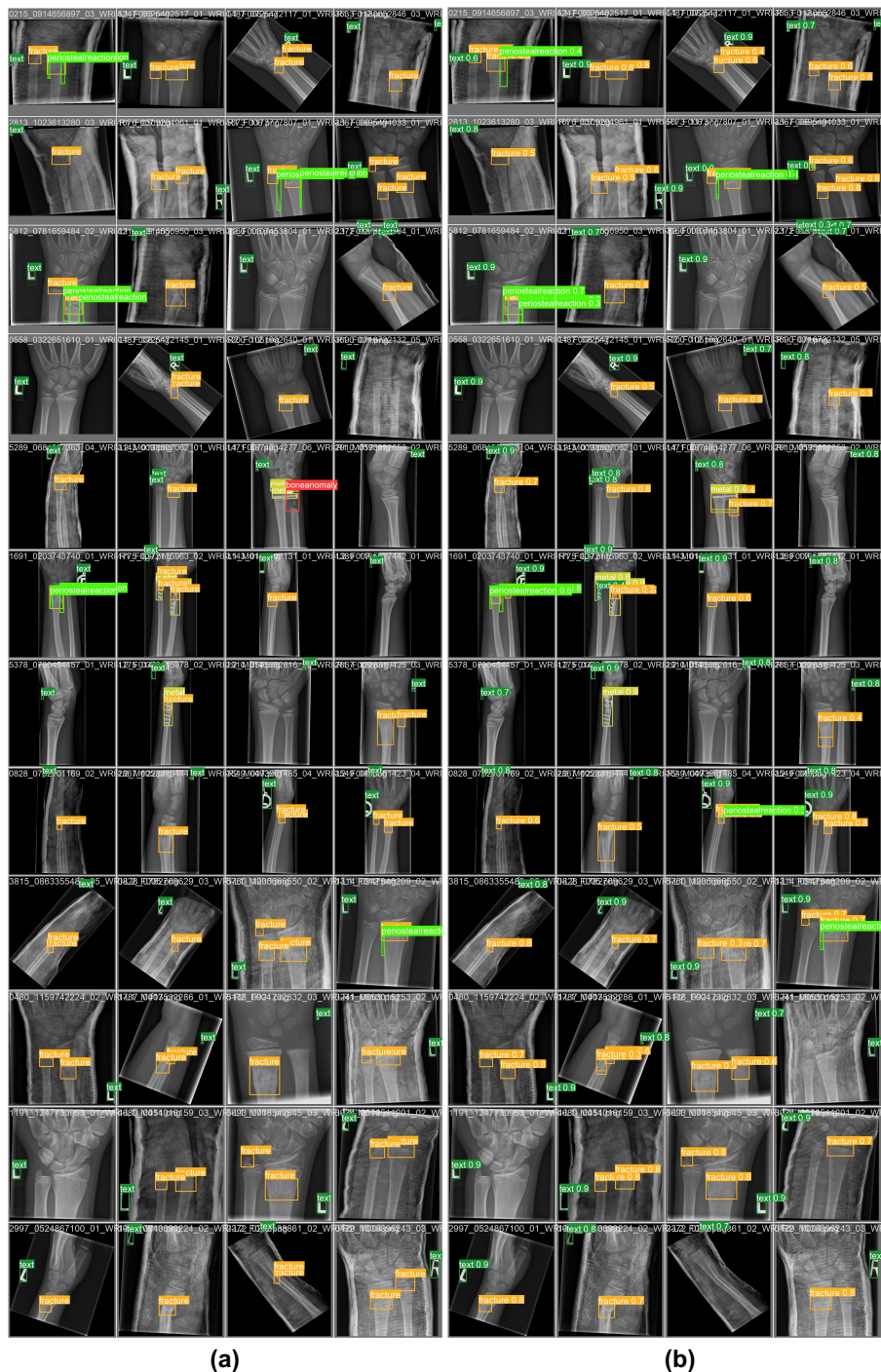


Fig. 4 Examples of the prediction of YOLOv8l model with the input image of 1024 in the GRAZPEDWRI-DX test set. (a) manually labeled images, (b) predicted images.

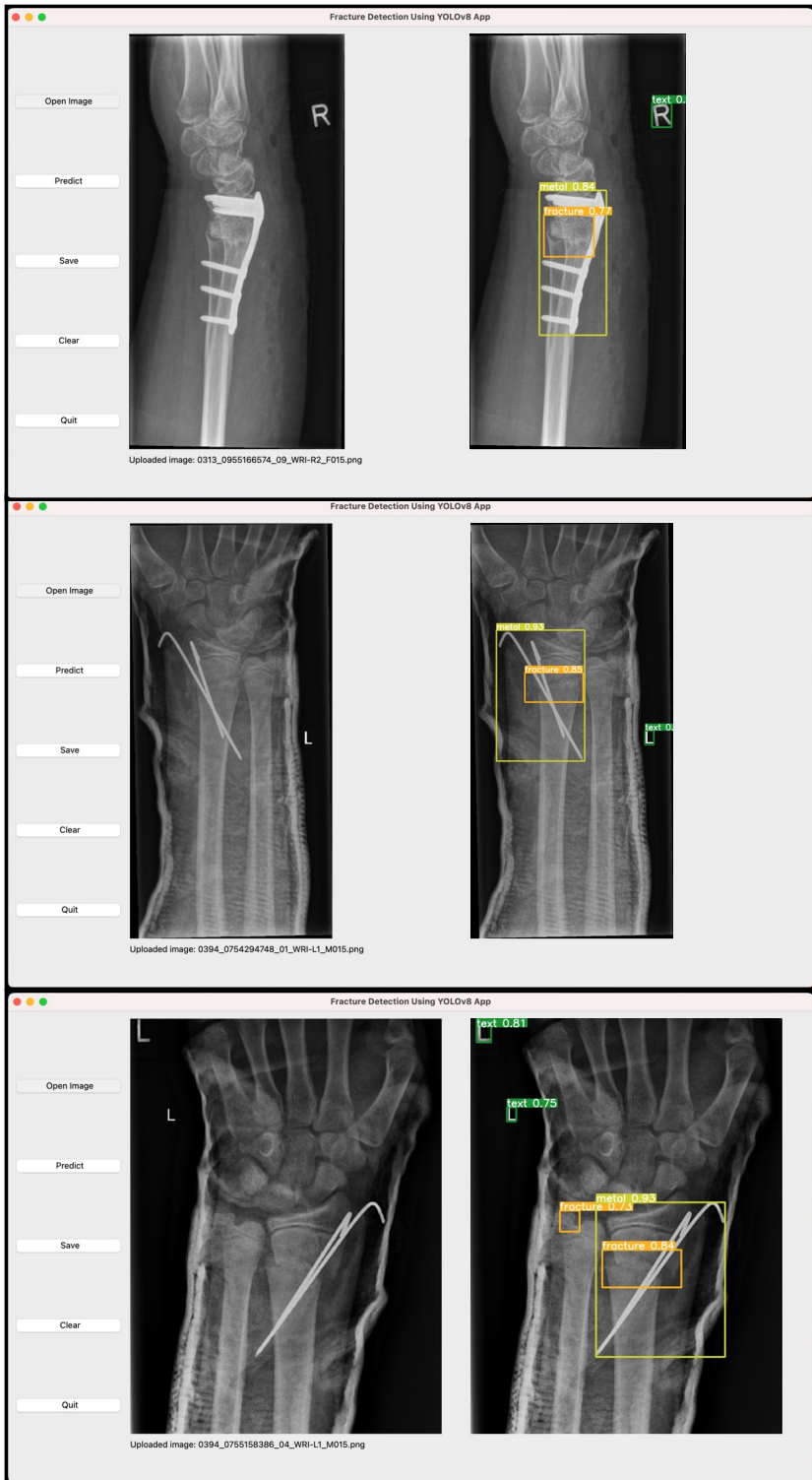


Fig. 5 Example illustration of the Graphical User Interface of the Fracture Detection Using YOLOv8 App.